J Electroceram (2009) 23:169–174
DOI 10.1007/s10832-007-9351-8

Effects of oxygen partial pressure on the preferential orientation and surface morphology of ITO films grown by RF magnetron sputtering

Jae-Hyung Kim · Joon-Hyung Lee · Young-Woo Heo · Jeong-Joo Kim · Ju-O Park

Received: 31 May 2007 / Accepted: 15 October 2007 / Published online: 1 November 2007
© Springer Science + Business Media, LLC 2007

Abstract In this study, effects of oxygen pressure in the sputtering ambient on the preferential orientation and resultant surface morphology of ITO films grown by RF magnetron sputtering were investigated. ITO film grown with pure Ar gas shows a preferential (400) plane orientation parallel to the substrate surface and a sawteeth-shaped rough surface. ITO film grown in the sputtering ambient of Ar and oxygen mixtures shows a preferential (222) plane orientation and a flat and smooth surface. The differences in the growth rate, surface morphology, and roughness between the preferentially orientated films were discussed in terms of the surface energy of planes. The electrical and optical properties of the films were examined.

Keywords ITO · RF magnetron sputtering
Surface morphology · Oxygen partial pressure

1 Introduction

Sn-doped In_2O_3 (indium tin oxide: ITO) is the most widely used material for transparent electrodes due to its high electrical conductivity and high transparency in visible regions [1–4]. Due to these properties, ITO films have been applied in many display devices such as liquid crystal displays, plasma display panels and organic light emitting diodes (OLEDs).

The control of the surface morphology of ITO thin films is one of the most exacting processing concerns. Surface modifications of ITO films are generally conducted in order to obtain a smooth surface by physical and chemical surface treatments [5, 6]. It has been known that surface modification plays an important role in enhancing the electrical and optoelectrical efficiency of OLEDs [7].

There have been many studies on the preferential orientation and surface morphology of thin films [8–15]. However, most researchers focused on the observation and analysis of the preferential orientation using methods such as X-ray diffraction (XRD), scanning electron microscopy (SEM), transmission electron microscopy (TEM), etc. Thilakan et al. [8] reported that the crystal growth behavior of ITO films was dependent on the oxygen concentration in the film. Mergel et al. [9] found that the orientation texture of the ITO films changed from (400) to (622) dominant with an increase in oxygen flux. They explained this resulted from the dynamic incorporation and segregation of oxygen during film growth. The dependency of surface morphology and crystal quality of ITO films on oxygen partial pressure in the processing gas has been reported [10, 11]. It was also suggested that changes in the preferential orientation of ITO films could be due to other reasons, such as the variation in energy of the sputtered atoms [16] and the concentration of Sn in the ITO film [17]. Kamei et al. [18] reported that the different re-sputtering rates between the (400) and (222) planes of ITO film during film growth could have affected crystalline orientation. The preferential orientation and resultant surface morphology of ITO thin films, however, has not been fully understood yet.

In this study, the effects of oxygen pressure in the sputtering ambient on the preferential orientation and

J.-H. Kim · J.-H. Lee · Y.-W. Heo · J.-J. Kim (✉)
Department of Inorganic Materials Engineering,
Kyungpook National University,
Daegu 702-701, South Korea
e-mail: jjkim@knu.ac.kr

J.-O. Park
Department of Materials and Systems,
Korean 3rd Military Academy,
Youngcheon 770-849, South Korea

resultant surface morphology of ITO films grown by RF magnetron sputtering were investigated. These phenomena are discussed from the viewpoint of surface energy. The electrical and optical properties of the films are also reported.

2 Experimental procedure

An ITO target having 90 wt% In_2O_3–10 wt% SnO_2 was prepared by a general solid-state reaction method. In_2O_3 (99.99%) and SnO_2 (99.99%) powders were used as raw materials. The powders was formed into a 150 mm diameter disk by cold isostatic pressing at 300 MPa, and then sintered for 10 h at 1550 °C in an oxygen atmosphere. The apparent density of the target was 99.2% and the dimensions of the target were adjusted to 76 mm in diameter and a thickness of 5 mm. The substrate of the SiO_2-coated Corning 1737 glass was cleaned in acetone, methyl alcohol, and de-ionized water in that order by an ultra sonic cleaner, then dried with nitrogen gas.

The base pressure of the chamber was 1.0×10^{-6} Torr. ITO films were grown on SiO_2-coated Coring 1737 corning glass under various $Ar{:}O_2$ flow ratios. The working pressure during the growth of the films was fixed at 10 mTorr with an RF sputtering power of 50 W. Oxygen partial pressure in the sputtering ambient varied from pure Ar to $Ar{:}O_2$ flow ratios of 9:1, 8:2, 7:3, and 6:4. The distance between the target and the substrate was 4 cm. The deposition process was carried out for 40 min at 300 °C. The crystal structure of the film was investigated by an X-ray diffractometer (Rigaku, D/MAX-2200H) using Cu-Kα radiation and a four-circle X-ray diffraction (Philips X'pert Pro-MRD). The surface morphology of the films was observed with a scanning electron microscope (SEM; Hitachi, S-4100) and a scanning probe microscope (SPM; Nano Scope IIIa, Digital Instruments of America). Transmission electron microscope (TEM; Hitachi H-9000) studies were conducted to analyze the structure of the films. A Focused Ion Beam (FIB) was employed for the TEM sample preparation. Hall-effect measurements with the van der Pauw technique (EGK, HEM-2000) were conducted to examine electrical and optical properties (UV-VIS-NIR Spectrophotometer; Varian, CARY 5G) were also analyzed.

3 Results and discussion

Figure 1 shows X-ray diffraction patterns of ITO films grown by RF magnetron sputtering as a function of oxygen partial pressure in the sputtering ambient. The preferential orientations of the ITO films depended on the oxygen

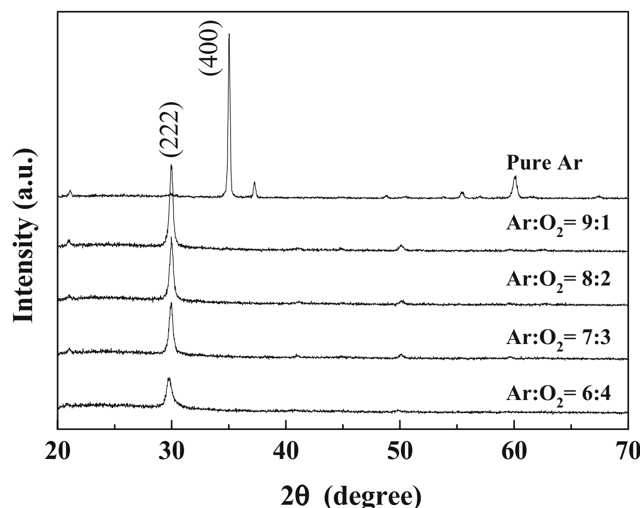

Fig. 1 X-ray diffraction patterns of ITO thin films as a function of oxygen partial pressure in the sputtering ambient

partial pressure. An ITO film grown with pure Ar gas shows a preferential (400) plane orientation parallel to the substrate surface. The preferential orientation of films changed from (400) to (222) plane when even a small amount of O_2 was added to the Ar sputtering ambient. It was also observed that the diffraction intensity of the (222) peak decreased as the oxygen partial pressure increased.

Figure 2 shows the (400) pole figure of preferentially (400) orientated films and the (222) pole figure of preferentially (222) orientated ITO films. The (400) pole figure of the former film indicates a well pronounced (400) texture, even though the (400) peak position is approximately 11° away from the normal direction (Fig. 2(a)). The <222> axis orientation of the preferentially (222) orientated film is perpendicular to the substrate surface (Fig. 2(b)). The (400) plane of preferentially (222) orientated ITO film is found approximately 55° away from the (222) normal, essentially the inter-plane angle of 54°44′ between the (400) and (222) planes of the body-centered cubic structure of the bixbyite ITO.

Cross sectional and tilted views of ITO thin films observed by SEM and AFM are presented in Fig. 3. The cross sectional views show that the thicknesses of the films significantly decrease when a small amount of oxygen is added to the sputtering ambient, and subsequently decreases slowly as the oxygen partial pressure increases. The thicknesses of the films were 625, 195, 130, 110 and 95 nm for pure Ar and $Ar{:}O_2$ flow ratios of 9:1, 8:2, 7:3 and 6:4, respectively. The gradual decrease in thickness with increase of the oxygen partial pressure can be explained by the smaller sputtering yields of oxygen ions than argon ions; the momentum transfer of oxygen is smaller than that of argon during ionic bombardment [19]. However, the thickness difference between the films that

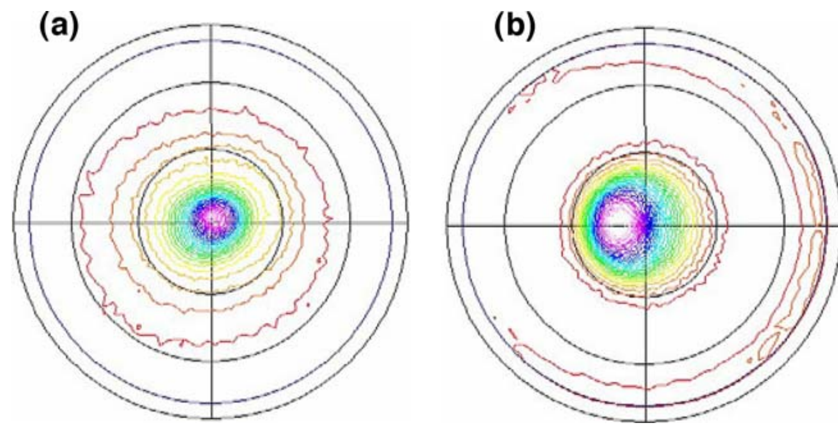

Fig. 2 Two dimensional pole figures through (**a**) (400) plane for the preferentially (400) orientated ITO thin film (*pure Ar*), and (**b**) (222) plane for the preferentially (222) orientated ITO thin film (*$Ar:O_2$= 9:1*)

are grown with and without oxygen is too significant to be explained only by the momentum transfer process. There must be additional reasons for that which will be discussed later in this work. Concerning the surface morphology in the tilted SEM photographs shown in Fig. 3, a very rough surface was observed in the (400) films while the (222) films revealed a smooth surface. RMS (root mean square) roughness was estimated by AFM surface analysis for the (400) film without oxygen and the (222) film grown with the $Ar:O_2$ ratio of 9:1 to be 4.2 and 0.8 nm, respectively. Smooth surface roughness was observed for other films grown with oxygen in the sputtering ambient. The RMS roughness of the films grown with the $Ar:O_2$ ratio of 8:2, 7:3 and 6:4 was 0.8, 0.8 and 0.7 nm, respectively. The surface roughness and thickness of the films were almost the same when oxygen was added ($Ar:O_2$ flow ratios of 9:1, 8:2, 7:3, and 6:4).

Concerning the momentum transfer of oxygen, the resputtering effect has been studied in sputtering-assisted oxide thin film growth, in which negative oxygen ions are frequently formed [20–26]. Cuomo et al. suggested that if the value of $I - EA$ (I: ionization potential, EA: electron affinity) were less than 3.4 eV, they predicted a negative ion formation, and the presence of resputtering effects [22, 23]. A subsequent study by Kester et al. [24] showed that the negative ion resputtering became stronger as the $I - EA$ value decreased. However, it is believed that the resputtering effect could not interpret every phenomenon which occurs in oxide films since discrepancies in experimental results often exist between films deposited with different materials and conditions.

According to research by Kester et al. [25], which is one of the most frequently cited regarding the resputtering effect, the film thickness decreased linearly as oxygen partial pressure increased. However, in the case of this study, the thicknesses of the films drastically decreased when a small amount of oxygen was added to the sputtering ambient, and they subsequently decreased slowly as the oxygen partial pressure increased (thickness change is

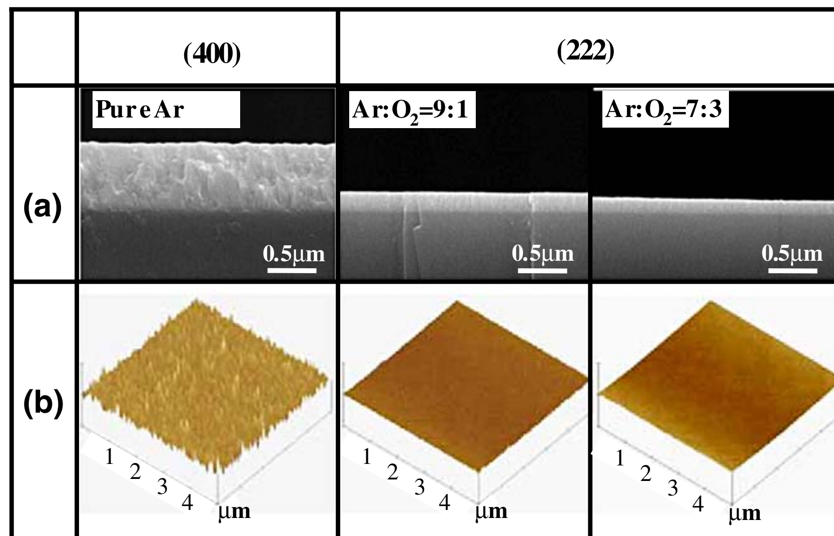

Fig. 3 (**a**) Cross-sectional SEM images and (**b**) three dimensional AFM images of ITO films grown as a function of oxygen partial pressure

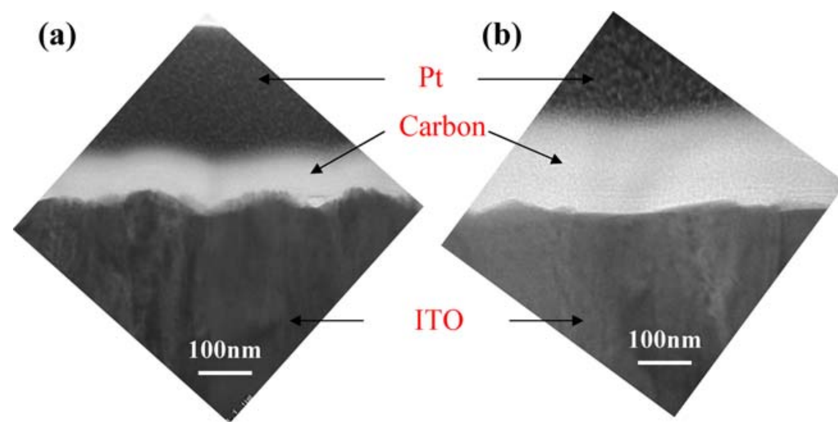

Fig. 4 TEM images of (**a**) the (400) and (**b**) (222) films

mentioned in Fig. 3). Concerning the surface roughness of the films, increase in the surface roughness was reported as the oxygen partial pressure increased due to the increase in the resputtering effect [18, 24]. This was not in agreement with our results also. When a small amount of oxygen was added, the roughness decreased from 4.2 (pure Ar) to 0.8 nm (Ar:O_2 ratio of 9:1). The further addition of oxygen did not greatly affect the surface roughness of the films as mentioned in Fig. 3, i.e., smooth surface roughness was observed for the films grown with oxygen in the sputtering ambient. Even though the $I - EA$ could not be an absolute standard value of resputtering, the $I - EA$ value of ITO was about 4.36 eV when the value was gathered from the previous studies [22–24], which signifies that the resputtering effect might not be such a serious problem in ITO system. From these points of view, even though resputtering might have partly contribute to ITO system, it has not predominantly affected the surface characteristics of ITO.

Figure 4 shows TEM images of the preferentially (400) oriented and (222) orientated ITO films. For TEM sample preparations using a Focused Ion Beam (FIB) milling and imaging system, carbon and platinum were sequentially deposited onto the film to sustain them during micro-machining. The white region on the film is the carbon followed by the platinum layer. The preferentially (400) oriented ITO film exhibited a sawteeth-shaped rough surface but the preferentially (222) orientated film showed a flat and smooth surface as shown in Fig. 4.

In order to explain the surface morphology of preferentially orientated films, the relationship between the surface energy of a given crystal plane and surface morphology was employed. Fig. 5 shows schematic drawings of the (400) and (222) planes in the bixbyite structure of ITO. The absolute surface energy of the (400) and (222) planes are not available either experimentally nor theoretically, but the relative surface energy of the planes can be compared by

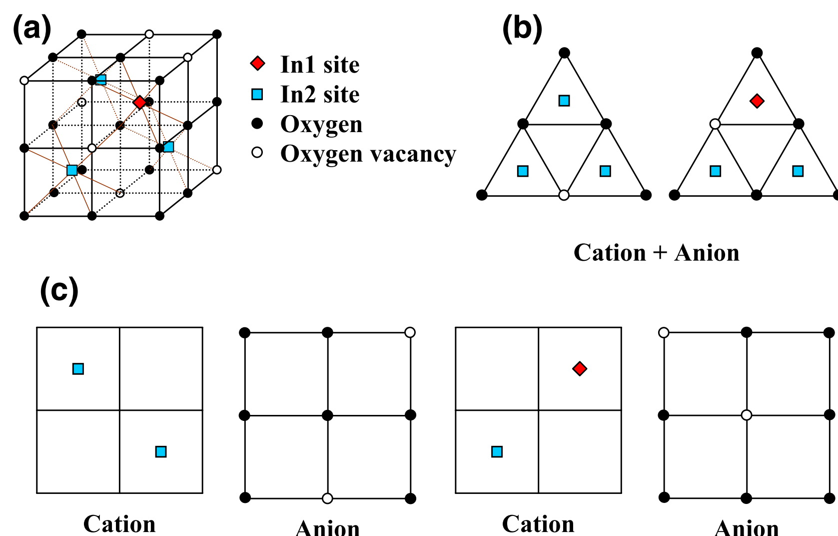

Fig. 5 Schematics of (**a**) In_2O_3 bixbyite structure and its (**b**) (222) and (**c**) (400) planes. Cations and anions coexist in the (222) plane, while either cations or anions exist in the (400) plane

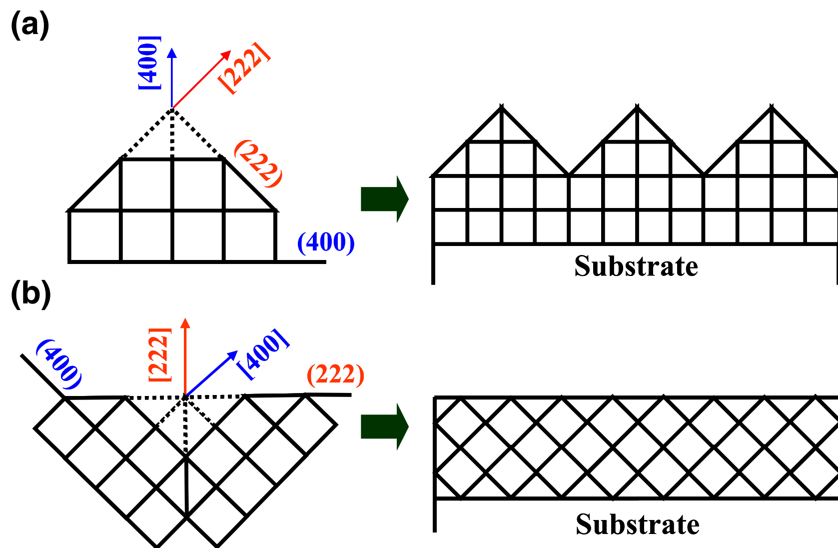

Fig. 6 Schematic diagrams of the crystallographic surface morphology of the preferentially (**a**) (400) and (**b**) (222) oriented films

considering the ratio of the cations and anions exposed on the surfaces. In the case of the (400) plane, either cations or anions are exposed to the (400) plane, while both cations and anions coexist on the closed-packed (222) plane. This indicates that the (400) plane has a higher surface energy than the (222) plane. Exposed surfaces of films have a tendency to be composed of planes having low surface energies to minimize the total surface energy [27]. It is therefore anticipated that the surface of the (400) oriented film will consist of energetically favorable (222) planes rather than (400) planes. This will result in sawteeth-shaped rough surface like the macroscopic facet as drawn in Fig. 6(a). The (222) oriented films, however, will have (222) planes parallel to the film surface, thus leading to a flat and smooth surface as drawn in Fig. 6(b). The observed surface morphologies of the preferentially (400) oriented and (222) oriented ITO films shown in Fig. 4 were consistent with the schematic drawings as shown in Fig. 6. As a consequence, the surface energy of the planes plays an important role in determining the surface morphologies of the preferentially oriented films.

When valleys, shaped by (222) planes as schematically drawn in Fig. 6(a), are formed on the surface of the (400) oriented film, they can provide preferential adsorption sites to which atoms are anchored. This, as well as the difference in the momentum transfer process of oxygen and argon previously mentioned, can lead to the faster growth rate of the (400) oriented films than the (222) oriented films.

The electrical properties of the films were analyzed by using Hall-effect measurements with the van der Pauw method. The results are summarized in Table 1. The carrier concentration, mobility, and resistivity are respectively 9.3×10^{20} cm^{-3}, 40.7 cm^2/V·s, 1.6×10^{-4} Ω·cm for the (400) films grown without oxygen and 3.2×10^{17} cm^{-3}, 8.5 cm^2/V·s, 2.2 Ω·cm for the (222) films grown with an Ar:O_2 ratio of 9:1. The higher carrier concentration of the ITO film without oxygen is in excellent agreement with the generation of electron carriers by oxygen vacancies in ITO. The difference in Hall mobility between the two films could be explained by the grain boundary scattering mechanism in the polycrystalline ITO films. The grain size of the (400) film is larger than that of the (222) films as shown in Fig. 3. It is not clear whether the different preferential orientation plays a role in variation of the Hall mobility of the films.

The average transmittance in the visible range for the films is above about 80%. The optical bandgap energy (E_g) for highly degenerated oxide semiconductors, in which direct transitions between the conduction band and the valence band occur, is obtained from the optical absorption coefficient near the absorption edge of $\alpha(h\nu - E_g)^{1/2}$ for $h\nu > E_g$, where α is the absorption coefficient [28]. The absorption coefficient α is calculated from transmission (T)

Table 1 Electrical and optical properties of ITO thin films.

Ar:O_2 ratio	Preferential orientation	Carrier concentration (cm^{-3})	Mobility (cm^2/V·s)	Resistivity (Ω·cm)	Optical bandgap (eV)	Work function (eV)
Pure Ar	(400)	9×10^{20}	41	1.7×10^{-4}	3.9	4.9
9:1	(222)	3×10^{17}	9	2.3	3.6	5.1

and reflection (R) measurements using the equation of $\alpha = (1/d)In\left[(1-R)^2/T\right]$, where d is the film thickness [28]. The optical bandgap energy is determined by the extrapolation of α^2 versus hν. The calculated optical band gap energy of the (400) film was 3.9 eV and that of the preferred (222) orientated film was 3.6 eV. The difference can be explained by the Burstein–Moss shift, which correlates the optical band gap shift with carrier concentration. The work function, measured by Ultraviolet Photoelectron Spectroscopy, revealed 4.9 and 5.1 eV for the (400) and (222) films, respectively. The higher work function in the (222) film is believed to be caused due to the lower carrier concentration in the conduction energy band as well as the smooth surface. The higher work function of (222) ITO film is more favorable to an increase in the hole injection at the ITO/polymer interface in polymer LEDs [29].

4 Conclusions

ITO thin films were grown by RF-magnetron sputtering with various oxygen partial pressures. The (400) ITO film grown in a pure Ar sputtering ambient showed a sawteeth-shaped rough surface that formed valleys in the macroscopic facets shaped by the low surface energy {222} planes. The (222) ITO film grown with oxygen has a flat and smooth surface that is formed by {222} planes parallel to the substrate surface. The differences in growth rate, surface morphology, and roughness between the preferentially orientated films were discussed in terms of the surface energy of crystal planes. The carrier concentration, mobility, conductivity, and optical bandgap energy of the (400) ITO films are higher than those of the (222) ITO films. The work function of the (222) ITO film is higher than that of the (400) ITO film.

Acknowledgements This work was supported by the Korea Research Foundation Grant funded by the Korean Government (MOEHRD) (KRF-2006-331-D00270).

References

1. I. Hamberg, C.G. Granqivst, J. Appl Phys. **60**, R123(1986)
2. S.J. Wen, G. Counturier, G. Campet, J. Portier, J. Claverier, Phys. Status Solidi **130**, 407(1992)
3. Y.-G. Park, K.-H. Seo, J.-H. Lee, J.-J. Kim, S.-H. Cho, C.J. O'Conner, J.-S. Lee, J. Electroceram. **13**, 851(2004)
4. S.-J. Hong, J.-I. Han, J. Electroceram. **17**, 821(2006)
5. M. Utsumi, N. Matsukaze, A. Kumagai, Y. Shiraishi, Y. Kawamura, N. Furusho, Thin Solid Films **363**, 13(2000)
6. S. Jung, N.G. Park, M.Y. Kwak, B.O. Kim, K.H. Choi, Y.J. Cho, Y.K. Kim, Y.S. Kim, Opt. Mater. **21**, 235(2003)
7. Ch. Jonda, A.B.R. Mayer, U. Stolz, A. Elschner, A. Karbach, J. Mater. Sci. **35**, 5645(2000)
8. P. Thilakan, C. Minarini, S. Loreti, E. Terzini, Thin Solid Films **388**, 34(2001)
9. D. Mergel, M. Schenkel, M. Ghebre, M. Sulkowski, Thin Solid Films **392**, 91(2001)
10. Y. Shigesato, D.C. Paine, Thin Solid Films **238**, 44(1994)
11. H. Ohta, M. Orita, M. Hirano, H. Hosono, J. Appl. Phys. **91**, 3547 (2002)
12. S. Choopun, R.D. Vispute, W. Noch, A. Balsamo, R.P. Sharma, T. Venkatesan, A. Iliadis, D.C. Look, Appl. Phys. Lett. **75**, 3947 (1999)
13. S. Kodambaka, S.V. Khare, V. Petrova, A. Vailionis, I. Petrov, J.E. Greene, Vacuum **74**, 345(2004)
14. C.S. Shin, D. Gall, Y.W. Kim, N. Hellgren, I. Petrov, J.E. Greene, J. Appl. Phys. **92**, 5084(2002)
15. S. Kodambaka, V. Petrova, A. Vailionis, O. Desjardins, D.G. Cahill, I. Petrov, J.E. Greene, Thin Solid Films **392**, 164(2001)
16. C.V.R.V. Kumar, A. Mansigh, J. Appl. Phys. **65**, 1270(1989)
17. C.H. Yi, I. Yasui, Y. Shigesato, Jpn. J. Appl. Phys. **34**, 600(1995)
18. M. Kamei, Y. Shigesato, S. Takaki, Thin Solid Films **259**, 38 (1995)
19. H.F. Winters, P. Sigmund, J. Appl. Phys. **45**, 4760(1974)
20. S.K. Park, J.H. Je, Physica C **254**, 167(1995)
21. O. Kappertz, R. Drese, J.M. Ngaruiya, M. Wuttig, Thin Solid Films **484**, 64(2005)
22. J.J. Cuomo, R.J. Gambino, J.M.E. Harper, J.D. Kuptsis, IBM J. Res. Dev. **21**, 580(1977)
23. J.J. Cuomo, R.J. Gambino, J.M.E. Harper, J.D. Kuptsis, J.C. Webber, J. Vac. Sci. Technol. **15**, 281(1978)
24. D.J. Kester, R. Messier, J. Vac. Sci. Technol. A **4**(3), 496(1986)
25. D.J. Kester, R. Messier, J. Mat. Res. **8**(8), 1928(1993)
26. D.J. Kester, R. Messier, J. Mat. Res. **8**(8), 1938(1993)
27. W.D. Kingery, H.K. Bowen, D.R. Uhlmann, *Introduction to Ceramics* (Wiley, New York (1976), 710–727
28. K.L. Chopra, S.R. Das, *Thin Film Solar Cells* (Plenum, New York (1983), 52–62
29. J.S. Kim, M. Granstrom, R.H. Friend, N. Johansson, W.R. Salaneck, R. Daik, W.J. Feast, F. Cacialli, J. Appl. Phys. **84**, 6859(1998)